

# Airfoil GAN: Encoding and Synthesizing Airfoils for Aerodynamic-aware Shape Optimization

Yuyang Wang, Kenji Shimada and Amir Barati Farimani  
*Department of Mechanical Engineering, Carnegie Mellon University, Pittsburgh, PA, 15213*

The current design of aerodynamic shapes, like airfoils, involves computationally intensive simulations to explore the possible design space. Usually, such design relies on the prior definition of design parameters and places restrictions on synthesizing novel shapes. In this work, we propose a data-driven shape encoding and generating method, which automatically learns representations from existing airfoils and uses the learned representations to generate new airfoils. The representations are then used in the optimization of synthesized airfoil shapes based on their aerodynamic performance. Our model is built upon VAEGAN, a neural network that combines Variational Autoencoder with Generative Adversarial Network and is trained by the gradient-based technique. Our model can (1) encode the existing airfoil into a latent vector and reconstruct the airfoil from that, (2) generate novel airfoils by randomly sampling the latent vectors and mapping the vectors to the airfoil coordinate domain, and (3) synthesize airfoils with desired aerodynamic properties by optimizing learned features via a genetic algorithm. Our experiments show that the learned features encode shape information thoroughly and comprehensively without predefined design parameters. By interpolating/extrapolating feature vectors or sampling from Gaussian noises, the model can automatically synthesize novel airfoil shapes, some of which possess competitive or even better aerodynamic properties comparing with training airfoils. By optimizing shape on learned features via a genetic algorithm, synthesized airfoils can evolve to have specific aerodynamic properties, which can guide designing aerodynamic products effectively and efficiently.

## Nomenclature

$z$	=	latent feature vectors of airfoils
$\hat{z}$	=	random noise sampled from Gaussian distribution
$x$	=	airfoils
$\tilde{x}$	=	airfoils reconstructed from $z$
$\hat{x}$	=	airfoils synthesized from $\hat{z}$
$\mathcal{L}_{prior}$	=	prior loss

$\mathcal{L}_{recon}$	=	reconstruction loss
$\mathcal{L}_{layer}$	=	layer like loss
$\mathcal{L}_{GAN}$	=	adversarial GAN loss
$C_l$	=	lift coefficient
$C_d$	=	drag coefficient

## I. Introduction

RECENT years have witnessed the success of deep learning [1] in many fields like computer vision [2], natural language process [3] and robotics [4] [5]. Such data-driven methods can automatically learn compact and comprehensive representations from samples. However, most of the prevalent deep learning models are based on supervised learning, meaning the samples are paired with manually tagged labels. Such supervision makes the model hard to generalize since both the amount of labeled data and the information contained in the label are limited. Hence, self-supervised learning is proposed to learn the features directly from data. Variational Autoencoder (VAE) [6] [7] follows the insight via an encoder-decoder structure, where the encoder down-samples high-dimensional input into a latent feature domain while the decoder reconstructs the sample from learned low-dimensional feature. By minimizing the difference between the reconstructed sample and the original one, VAE automatically learns features without any labels. Generative Adversarial Network (GAN) [8] pushes learning from self-supervision even further via a min-max game between a generator and a discriminator. The discriminator works as a classifier to determine real samples from synthesized fake ones; meanwhile, the generator which synthesizes samples from random noise is intended to cheat the discriminator. By jointly training the two components, GAN can generate super high-quality realistic samples [9], which VAE fails to achieve. Through learning to reconstruct or synthesizing samples, the self-supervised models automatically encode high-dimensional input into informative features, which can be generalized to different tasks without restrictions from human labels.

Such a self-supervised learning manner can help the parameterization of various geometries using the learned representations. Geometry parameterization plays an important role in shape design [10–12], and geometry heavily influences the performance, especially in the design of aerodynamic products like airfoils. A practical and effective airfoil design must meet certain aerodynamic requirements, like lift, drag, pitching moment, and critical-speed characteristics [13]. However, due to the curse of dimensionality, design optimization based on CFD simulations can be hard or even infeasible on the airfoil geometry domain, especially for gradient-free methods [14]. Therefore, parameterization or dimension-reduction is required to define the design domain before any design optimization is applied. Traditional parameterization or dimension-reduction techniques rely on manually selected design parameters like control points of Bézier curves [15] or B-splines [16], which places restrictions on the generalization to various shapes as well as

synthesizing novel geometries. Implementation of self-supervised deep learning methods on shape parameterization, like VAE and GAN, can overcome the limitations of traditional techniques and synthesize shapes with great novelty, which can provide insights for future geometric design.

In this work, VAEGAN [17], which is a combination of Variational Autoencoder (VAE) and Generative Adversarial Network (GAN), is utilized to learn feature vectors and generate novel airfoils without any human prior. VAEGAN takes advantage of both VAE and GAN. With the encoder-decoder architecture from VAE, the model learns to explicitly encode an existing airfoil shape into a low-dimensional feature domain and reconstruct the shape with little error. With the discriminator from GAN, our model can generate a large number of high-quality novel airfoils from random noise with no manually designed parameters.

Our experiments show that generated airfoils are smooth even without any smoothing post-process. K-means clustering in the learned feature domain demonstrates that feature vectors encode essential shape information in a way that each cluster represents various shape patterns. Further test on learned latent features illustrates that different geometry information is encoded in each dimension of the representation. The performance of the model in synthesizing novel airfoils is examined as well. By either interpolation or extrapolation of feature vectors, a synthesized airfoil inherits features of parent samples, while generated airfoils from sampled Gaussian noise show great novelty in a way that it is not a simple combination of two existing airfoils. A further experiment on the aerodynamic properties of synthesized airfoils, either by interpolating, extrapolating, or sampling, indicates the synthesized airfoils can possess competitive aerodynamic properties, and some even surpass the existing ones. With a genetic algorithm [18], airfoil geometries can be optimized on the feature domain and evolve to possess specific aerodynamic properties. Our model proves its ability to parameterize the existing airfoil shape as well as generating novel and practical airfoils; both lead to designing the new generation of airfoils more intelligently and efficiently without intensely relying on experimental experience or manually design parameters.

## **II. Related Works**

We propose to use a generative model to synthesize novel airfoils without any predefined design parameters. Through training via the gradient-based method, our deep learning model also automatically learns to parameterize airfoils into latent feature vectors. To better address the insight of our work, this section reviews previous work on shape parameterization, especially on aerodynamic geometries and the implementation of deep learning on geometry design and synthesis.

### **A. Geometry Parameterization and Dimension Reduction**

A lot of work has been done in parameterizing complex shapes and reducing geometric dimensions. Some research focuses on analytically expressing the curves. In [19], it is introduced that by adding analytic shape functions to the

baseline shape, a compact formulation for parameterization can be obtained. The design variables, in this case, are the coefficients correlated with shape functions. By this means, the analytical function of the airfoil curve is formulated. Also, [20] follows the same formulation strategy but with different shape functions. Another common and efficient method is PARSEC [21], which defines eleven geometric parameters to thoroughly express the airfoil shape, including upper and lower curvature, thickness, leading-edge radius, etc. With the defined parameters, a linear combination of shape functions is introduced to describe the airfoil shape as well. Such methods work well for a specific set of curves but may fail to express complex geometries since they rely on manually designed parameters.

Polynomial and spline are also utilized to help dimension reduction. With different orders of polynomials as the basis, the airfoil shape can be described as a linear combination of the basis [22, 23]. However, high-order terms can overfit to high-frequency noise, especially when coefficients are of different magnitudes. Besides polynomial, Bézier curve [15], which is built upon the Bernstein polynomials, is another mathematical formulation of curves. In detail,  $n + 1$  control points of Bézier are needed to define an  $n$ -degree Bézier curve. Although Bézier and polynomial curves are mathematically equivalent, Bézier usually perform better in controlling a curve since control points are closely related to the curve position and shape. To mitigate the rounding error, De Casteljaou [24], a recursive algorithm, is introduced to compute the Bernstein polynomials numerically. Besides, Bézier-PARSEC [16], which combines Bézier and PARSEC, uses PARSEC parameters to define Bézier curves. The B-spline curve with B-spline basis functions is also utilized to describe the airfoil shape. Yet B-spline formulation fails to represent implicit conic sections accurately. That is why Non-uniform rational B-spline (NURBS) is introduced [25]. NURBS can accurately represent both standard geometric objects like lines, circles, ellipses, and cones, as well as free-form geometry, which are prevalent in industrial design.

Another popular technique in shape parameterization is free-form deformation (FFD), which utilizes high-level shape deformation instead of lower-level geometric entities to represent a shape. Based on this insight, [26] presents a technique which can apply deformation either locally or globally based on trivariate Bernstein polynomials. Deformation is manipulated by control points of trivariate Bézier volumes. In [27], an extended free-form deformation (EFFD) method is presented, which allows arbitrarily shaped deformations by using non-parallelepiped lattices. Research presented in [28] incorporates FFD and sensitivity analysis where geometry changes and structural responses are correlated, and the shape satisfying deformation or stress constraints can be found easily.

Other methods like leveraging camber and thickness mode shapes derived from existing airfoils are also used to parameterize the airfoil shapes [29]. Also, the linear reduction method like the SVD is utilized to extract airfoil representations and optimize shape design [30]. The conventional dimension reduction or parameterization techniques have been implemented in different scenarios and successfully represented the existing airfoil shapes. However, these methods usually require pre-defining the design space as well as the boundary of design space, like the design parameters in NACA, shape functions, etc., which can degrade the synthesis of novel/new airfoils and optimization towards the desired design.”

## B. Deep Learning in Geometry Design

In recent years, deep learning has been a great success in extracting informative features from data [1]. Especially in a supervised visual learning manner, with the invention of convolutional neural network (CNN) [31, 32], deep learning has been general solutions in many fields, like image classification [33] [34], object detection [35, 36], and segmentation [37, 38]. Also, with the introduction to GAN [8], deep learning in a self-supervised manner has been widely used in synthesizing realistic samples, and some sophisticated GAN-based model can generate high-resolution images which are even hard to distinguish by humans [9]. With the ability to extract representative features and synthesize realistic samples, deep learning has been widely used to make geometric design more systematic and efficient. This section will introduce some work of deep learning in geometric design, especially in aerodynamic shape design.

In the work of [39], a multi-layer perceptron (MLP), which takes the angle of attack and flap setting as input, is trained to predict multiple aerodynamic coefficients, including lift coefficient, drag coefficient, and moment of inertia. Further, [40] utilizes CNN with airfoil images as input to learn the lift coefficients of different airfoils in multiple flow Mach numbers, Reynolds numbers, and diverse angles of attack. Similarly, in [41], CNN is implemented to predict the pressure coefficient value at the test point. Moreover, [42] presents a CNN-based method to learn the correlation between airfoil geometry and pressure distribution. The model can also conduct an inverse airfoil design given the pressure.

On the other hand, the GAN model [8], as a self-supervised learning framework, has been a prevalent and great success in generating realistic samples. GAN, with a discriminator and a generator, is designed to learn features and generate samples without manually tagged labels. The discriminator is a classifier telling the true input from the synthesized fake one, while the generator is intended to generate plausible samples to cheat the discriminator. Since first introduced [8], many pieces of research have been dedicated to pushing the edge of GAN. In Wasserstein GAN [43], by introducing Wasserstein distance, the quality of generated samples can be well measured during training. ConditionalGAN [44] and InfoGAN [45] extend GAN to generate a sample from various categories within one model. Also, DCGAN [46] and StyleGAN [9] can generate high-quality realistic samples with sophisticated architectures.

With the ability to generate plausible samples, GAN provides a powerful architecture to learn representations that can help shape design as well. Based on this insight, [47, 48] introduce BézierGAN, which uses a GAN to generate Bézier curve control points and then uses the control points to formulate the boundary of airfoils. Such pipeline guarantees generated airfoils to be smooth, and further shape optimization can be conducted on the feature domain [48]. Such a method is, however, restricted to Bézier curves and fails to encode existing airfoil shapes explicitly. Further, GAN can be implemented in generating three-dimensional samples, as shown in [49–51]. [49] proposes to use a three-dimensional convolutional layer to generate volumetric objects. While [50] trains a generative model of three-dimensional shape surfaces, which directly encodes surface geometry and shape structure, [52] further proposes a model to represent probabilistic relationships between properties of shape components and relates them to learned underlying causes of

structural variability within the domain.

In our work, we propose to use a VAEGAN-based model [17] to extract features of airfoil shapes and synthesize new airfoil designs. The learned latent features encode the airfoil shape and can be utilized to synthesize new designs through interpolation or extrapolation. In comparison to conventional parameterization methods, our model can generate a wider variety of new airfoils, and some show promising aerodynamic properties. By applying the genetic algorithm, the VAEGAN synthesized airfoils can be optimized to desired aerodynamic properties.

### III. Proposed Method

#### A. Data Pre-processing

The UIUC Coordinates Database [53], which contains more than 1,600 2-dimensional airfoils, is used to train the generative model. Each airfoil in the database is represented by varying numbers of points with x, y coordinates. Such variation restricts data to be fed directly into a neural network model, which requires a homogeneous input. To deal with it, we first scale the x coordinates of all airfoils to [0, 1]. Then all airfoils are interpolated by splines, and  $N$  points are selected with  $x$  given in Eq. 1, where  $i$  represents the index of each point.

$$\begin{aligned} \theta_i &= \frac{\pi(i-1)}{N} \\ x_i &= 1 - \cos(\theta_i) \end{aligned} \tag{1}$$

In our case,  $N$  is set to be 200 with 100 points from the upper boundary and the other 100 from the lower boundary. By this means, all the interpolated airfoils share the same x coordinates. Therefore, only the y coordinates of each airfoil are fed into the model, which reduces the dimensionality of the data. Finally, all y coordinates are scaled to  $[-1, 1]$  by multiplying a normalization coefficient. As illustrated in Fig 1, the first row shows the original airfoils from the UIUC Coordinate Database, while the second row shows the corresponding processed airfoils.



**Fig. 1 Data pre-processing: the first row shows the origin airfoil coordinates from the UIUC database, the second row shows the corresponding processed airfoils**

#### B. VAEGAN

Our model is based upon VAEGAN [17], which takes advantage of both VAE [6] [7] and GAN [8]. VAE contains two components: an encoder and a decoder. The former encodes a high-dimensional sample,  $x$ , into a low-dimensional

latent representation,  $z$ . While the decoder takes as input the latent vector,  $z$ , and upsamples from the representation domain to the original data domain,  $\tilde{x}$ . The encoder and decoder are given as:

$$z \sim \text{Enc}(x) = q(z|x), \tilde{x} \sim \text{Dec}(z) = p(\tilde{x}|z). \quad (2)$$

To regularize the encoder, VAE takes into consideration a prior distribution of the latent vector,  $p(z)$ . Here it is assumed that  $z \sim \mathcal{N}(0, \mathbf{I})$ , which follows an isotropic Gaussian distribution. The loss function for VAE to minimize is given by:

$$\mathcal{L}_{VAE} = \mathcal{L}_{recon} + \mathcal{L}_{prior}, \quad (3)$$

with

$$\begin{aligned} \mathcal{L}_{recon} &= \|\tilde{x} - x\|_2^2, \text{ and} \\ \mathcal{L}_{prior} &= D_{KL}(q(z|x)||p(z)), \end{aligned} \quad (4)$$

where  $\mathcal{L}_{recon}$  measures how well the reconstructed data,  $\tilde{x}$ , is comparing to the original  $x$  by the mean square error (MSE), and  $\mathcal{L}_{prior}$  is the Kullback Leibler divergence (KL divergence), which measures the difference between encoded representation vectors and Gaussian distribution.

VAE learns the representation of samples and can reconstruct them from  $z$  with the encoder-decoder architecture. However, it suffers from poor performance in generating novel samples, which have not been seen before [8] [17]. To this end, a generative adversarial network (GAN) [8] is introduced, which contains a discriminator,  $\mathcal{D}$ , and a generator,  $\mathcal{G}$ , competing with each other in a self-supervised manner.  $\mathcal{G}$  tries to generate plausible samples to fool  $\mathcal{D}$ , while  $\mathcal{D}$  keeps sharpening its decision boundary to determine synthesized fake samples from real ones. In detail, the generator,  $\mathcal{G}$ , is fed with random noise  $\hat{z} \sim p(\hat{z})$  and maps the noise to the data sample domain to generate fake  $\hat{x}$ . The discriminator takes both  $x$  and  $\hat{x}$  to predict whether the input is from the real dataset or generated by  $\mathcal{G}$ . The cross-entropy loss function for the min-max game is given as:

$$\min_G \max_D \mathcal{L}_{GAN} = \log \mathcal{D}(x) + \log(1 - \mathcal{D}(\mathcal{G}(\hat{z}))). \quad (5)$$

As one may expect, GAN generates samples purely from random noise, making it hard to obtain an explicit mapping from the data domain to the feature domain. Therefore, we build our model upon VAEGAN, which combines VAE and GAN. Namely, the generator is replaced by an encoder-decoder structure from VAE, as shown in Figure 2. Notice that in VAEGAN, the model generates a reconstructed sample,  $\tilde{x}$ , given a real sample,  $x$ , and meanwhile generates a fake sample,  $\hat{x}$ , directly from noise,  $\hat{z}$ . Both  $\tilde{x}$  and  $\hat{x}$  should be classified as fake by the discriminator,  $\mathcal{D}$ , and only  $x$  is

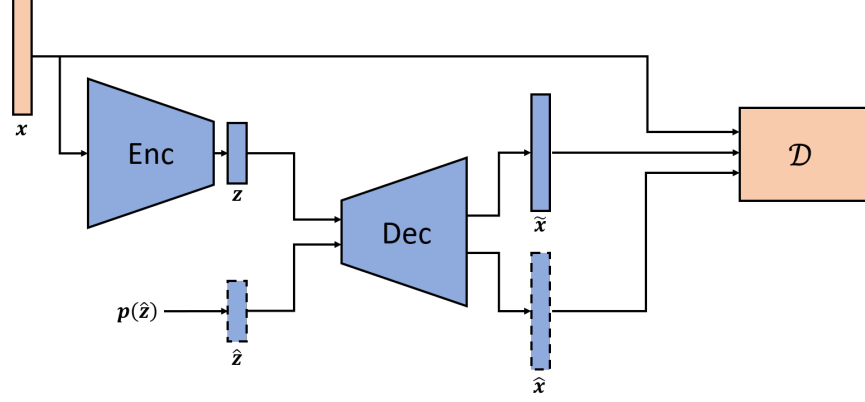


**Fig. 2** VAEGAN combines the encoder-decoder structure from VAE and discriminator,  $\mathcal{D}$ , from GAN

recognized as the real sample. Hence GAN loss function  $\mathcal{L}_{GAN}$  from Eq. 5 is modified to:

$$\mathcal{L}_{GAN} = \log(\mathcal{D}(x)) + \log(1 - \mathcal{D}(\text{Dec}(z))) + \log(1 - \mathcal{D}(\text{Dec}(\text{Enc}(x)))), \quad (6)$$

which takes into consideration the real sample,  $x$ , reconstructed sample,  $\tilde{x}$ , and fake sample,  $\hat{x}$ . Besides, to stabilize the training process and sharpen the decision boundary of  $\mathcal{D}$ , another loss function,  $\mathcal{L}_{layer}$ , is introduced when training the encoder and decoder.  $\mathcal{L}_{layer}$ , as given in Eq. 7, measures the  $l_1$  distance between the values of the neurons in one particular layer of  $\mathcal{D}$  when fake samples are fed and the values when real samples are fed.

$$\mathcal{L}_{layer} = \|\mathcal{D}_l(x) - \mathcal{D}_l(\text{Dec}(\hat{z}))\|_1. \quad (7)$$

The complete loss function for VAEGAN is a weighted combination of all the loss terms given by:

$$\mathcal{L} = \lambda_0 \mathcal{L}_{prior} + \lambda_1 \mathcal{L}_{recon} + \lambda_2 \mathcal{L}_{layer} + \lambda_3 \mathcal{L}_{GAN}. \quad (8)$$

The three components, encoder, decoder and discriminator are trained jointly, and each term of the loss function is assigned with different weights  $\lambda$  when training each component.

### C. Airfoil Synthesis

By training on the UIUC Database, the VAEGAN model automatically learns to encode airfoils into latent features and reconstruct airfoils from the feature domain. The learned latent features can be directly utilized for dimension reduction and shape parameterization. Moreover, the VAEGAN model is intended to synthesize novel airfoils which are different from samples in the training dataset. To this end, we propose three synthesis methods: interpolation, extrapolation, and sampling, all of which are conducted on the latent feature domain.



More specifically, in interpolation or extrapolation, two airfoils from the UIUC Database are first mapped to latent feature vectors,  $z_1$  and  $z_2$ , via a well-trained encoder. A new feature vector  $\bar{z}$ , which is an affine combination of  $z_1$  and  $z_2$ , is calculated as given in Eq. 9:

$$\bar{z} = \nu z_1 + (1 - \nu) z_2, \quad (9)$$

where  $\nu$  is the coefficient controlling the weight between  $z_1$  and  $z_2$ . When  $0 \leq \nu \leq 1$ ,  $\bar{z}$  is an interpolated feature vector, else it is an extrapolation between  $z_1$  and  $z_2$ . The interpolated/extrapolated feature vector,  $\bar{z}$ , is then fed into the decoder to synthesize an airfoil. Also, such interpolation/extrapolation between two airfoils can be directly extended to a triplet case. Given  $z_1$ ,  $z_2$ , and  $z_3$  are three feature vectors mapped from three different airfoils via the encoder, the expression of triplet interpolation/extrapolation is shown in Eq. 10:

$$\bar{z} = \alpha z_1 + \beta z_2 + \gamma z_3, \text{ where } \alpha + \beta + \gamma = 1. \quad (10)$$

Similarly, when  $0 \leq \alpha, \beta, \gamma \leq 0$ ,  $\bar{z}$  is an interpolation of the three feature vectors, and an extrapolation otherwise.

Besides interpolation and extrapolation, sampling is another method to synthesize novel airfoils. Unlike interpolation or extrapolation, which relies on feature vectors from existing airfoils, sampling generates airfoils directly from random noise. A feature vector  $\hat{z}$  is randomly sampled from an isotropic Gaussian distribution  $\mathcal{N}(0, \mathbf{I})$  and then mapped to an airfoil via the decoder. By this means, synthesized airfoils from sampling are less restricted since sampled latent vectors are not constrained by features extracted from airfoils in the UIUC Database and are more likely to introduce novelty to the synthesized shapes.

#### D. Aerodynamic-aware Shape Optimization

So far, how the VAEGAN model is built and used to generate novel airfoils has been introduced. However, the novelty in shape does not guarantee a better airfoil design. To design engineering effective airfoils, aerodynamic properties are supposed to be considered. To this end, we propose to use a genetic algorithm (GA) [54] [18] to optimize airfoil shapes by controlling feature vectors learned from the VAEGAN model so that the airfoils can evolve to have the desired aerodynamic properties. Specifically, lift coefficient,  $C_l$ , and drag coefficient,  $C_d$ , which measure the aerodynamic force perpendicular and horizontal to the direction of motion, are considered to evaluate the aerodynamic performance of the synthesized airfoils.

As a non-gradient optimization technique, GA is inspired by natural selection and is intended to force individuals to gradually evolve to the optimal. Assume the GA has  $N$  generations in total and  $M$  individuals in each generation. In our case, individuals are feature vectors. We use  $z_i$  to represent all individuals in the  $i^{\text{th}}$  generation, and  $z_{i,j}$  for the  $j^{\text{th}}$  individual in the  $i^{\text{th}}$  generation; also the airfoil decoded from  $z_{i,j}$  is annotated as  $a_{i,j}$ . Similarly,  $C_l^{i,j}$  and  $C_d^{i,j}$  represents lift and drag coefficients of  $a_{i,j}$ , respectively. The fitness score,  $s_{i,j}$ , is used to measure the aerodynamic performance of

the individual,  $z_{i,j}$ , as shown in Eq. 11:

$$s_{i,j} = -\left(\frac{C_l^{i,j} - C_l^t}{C_l^t}\right)^2 - \left(\frac{C_d^{i,j} - C_d^t}{C_d^t}\right)^2, \quad (11)$$

where the square of the difference between the target and current aerodynamic coefficients is calculated and normalized by the squared target  $C_l^t$  and  $C_d^t$ . The fitness score is supposed to approach zero as individuals evolve on each generation. As shown in Algorithm 1, the initial generation,  $z_0$ , is randomly sampled from an isotropic Gaussian distribution,  $\mathcal{N}(0, \mathbf{I})$ . The GA starts with the selection from the initial generation by randomly picking two individuals and comparing their fitness scores. The one with a higher fitness score wins the tournament and becomes one of the parents.  $p_1^i$  and  $p_2^i$  denote all the parents 1 and parents 2 in the  $i^{\text{th}}$  generation respectively. Single-point crossover is then implemented to generate offspring from parents 1 and 2. Namely, a crossover point on the parent vector is randomly selected, and all elements after that point are swapped between the two parents. Mutation in the natural selection process is also imitated with additive Gaussian noises.

---

**Algorithm 1** Aerodynamic-aware Shape Optimization via GA

---

```

1: procedure GA( $N, M, C_l^t, C_d^t, p$ )
2:   Initialize  $i := 0$ 
3:   Sample first generation  $z_{0j} \sim \mathcal{N}(0, \mathbf{I})$ , for  $0 < j < M$ 
4:   while  $i < N$  do
5:     Synthesize airfoils  $a_{i,j}$  from  $z_{i,j}$  via decoder
6:     Compute  $C_l^{i,j}, C_d^{i,j}$  and fitness score  $s_{i,j} = -\left(\frac{C_l^{i,j} - C_l^t}{C_l^t}\right)^2 - \left(\frac{C_d^{i,j} - C_d^t}{C_d^t}\right)^2$ 
7:     Select  $M$  parent 1,  $p_1^i$ , and  $M$  parent 2,  $p_2^i$ , from  $z_i$  by tournament
8:     Generate next generation,  $z_{i+1}$ , through single-point crossover
9:     With probability  $p$ ,  $z_{i+1,j}$  will add a Gaussian noise  $\mathcal{N}(0, \mathbf{I})$ 
10:    return  $i := i + 1$ 
    return The individual with the highest score from  $z_i$ 

```

---

## IV. Experiments

Our VAEGAN model consists of 3 components: an encoder, a decoder, and a discriminator, which are all built on multi-layer perceptron (MLP). As illustrated in Fig 2, the encoder encodes 200-dimensional airfoil coordinates into a 32-dimensional feature domain while the decoder maps the feature back to the airfoil. The discriminator is a classifier examining whether the input is a real airfoil from the UIUC Database, or a fake one reconstructed from the decoder, or synthesized from random noises. In detail, the encoder is modeled by a 3-layer MLP with the number of neurons [256, 128, 32] in each layer, and LeakyReLU [55] is implemented as the activation function in each layer. The decoder is also a 3-layer MLP with the number of neurons [128, 256, 200] in each layer. A hyperbolic tangent (Tanh) function works as the activation function in the output layer to scale all outputs into  $[-1, 1]$ . Similarly, the discriminator contains three layers with the number of neurons [256, 128, 1], and outputs the probability of whether the input is real or fake

through a Sigmoid activation function.

To automatically learn the latent features and synthesize airfoils, the VAEGAN model is trained on the UIUC Database for 5000 epochs, and each epoch goes through all the samples in the dataset. Initial learning rates for all three components: encoder, decoder, and discriminator are set to be 0.0005 and decay to 0.00005 after 2500 epochs. The batch size is set to be 16, which is approximately 1/100 of the database size. Adam optimizer [56] is utilized to update all the parameters in the model. As mentioned in Section III C, different coefficients are assigned to each term in the loss function Eq. 8; also different components, namely the encoder, decoder, and discriminator, have different coefficients, respectively. Coefficients of different loss terms and components are shown in Eq. 12:

$$\begin{aligned}\mathcal{L}_{Enc} &= 0.1\mathcal{L}_{prior} + 0.1\mathcal{L}_{layer} + 10\mathcal{L}_{recon}, \\ \mathcal{L}_{Dec} &= 0.1\mathcal{L}_{prior} + 0.1\mathcal{L}_{layer} + 10\mathcal{L}_{recon} + 5\mathcal{L}_{GAN}, \\ \mathcal{L}_{\mathcal{D}} &= \mathcal{L}_{GAN},\end{aligned}\tag{12}$$

where  $\mathcal{L}_{Enc}$ ,  $\mathcal{L}_{Dec}$ , and  $\mathcal{L}_{\mathcal{D}}$  represent loss functions for the encoder, decoder, and discriminator, respectively.

To better investigate our VAEGAN-based model, we compare the performance with two other parameterization methods, principle component analysis (PCA) and variational autoencoder (VAE) [6]. PCA conducts a linear transformation from the pre-processed airfoil point coordinates into prioritized latent variables. In our case, the top 32 dimensions are kept as the feature. The VAE follows the same encoder-decoder architecture as the VAEGAN, but lacks the discriminator. The latent feature dimension is also set to 32, and the loss function is given in Eq. 13:

$$\mathcal{L}_{Enc} = 0.1\mathcal{L}_{prior} + 10\mathcal{L}_{recon}.\tag{13}$$

#### A. Airfoil Reconstruction via Encoder-decoder

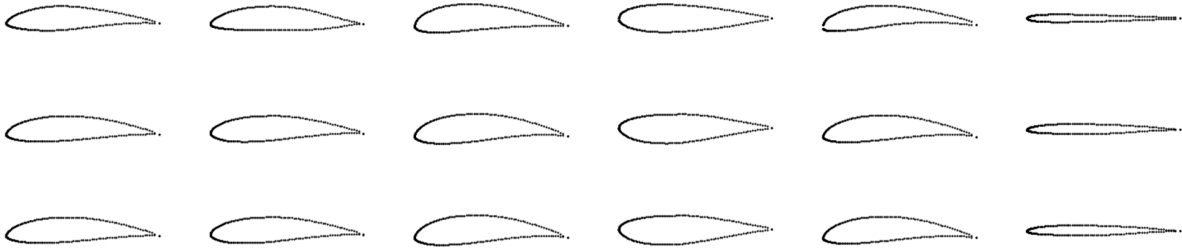


**Fig. 3 Reconstructed airfoils: the first row shows the airfoils from UIUC Coordinate Database, the second row shows the reconstructed airfoils with VAE, and the third row shows the reconstructed airfoils with smoothness**

The VAEGAN model can automatically learn feature vectors, namely mapping the high-dimension airfoils into

low-dimension representations. To estimate whether or not the feature vector fully encodes the geometric information of the original airfoil, we first feed airfoils from UIUC Coordinate Database into the encoder to obtain the encoded feature vectors. The decoder then takes the vectors as input and outputs the reconstructed airfoils. Also, the Savitzky-Golay filter [57], a moving polynomial fitting, is implemented to smoothen the boundary of reconstructed airfoils. In our case, the second-order polynomial is used in the Savitzky-Golay filter, and the length of the moving window is set to be 7. In Fig 3, the first row illustrates samples from the UIUC Database, and the second row shows reconstructed airfoils from corresponding feature vectors, with an MSE,  $3.65345 \times 10^{-4}$ , between the reconstructed and original airfoils. This small error indicates the learned features well represent the shape of airfoils. The third row shows reconstructed airfoils with the Savitzky-Golay filter with an MSE,  $3.65054 \times 10^{-4}$ , comparing to the original airfoils. These results further demonstrate that the encoder-decoder can reconstruct airfoils that are smooth and realistic without smoothing filters. Also, our VAEGAN-based model is compared with PCA and VAE as shown in Table 1. PCA reaches the lowest MSE since it provides a close form solution, whereas VAE and VAEGAN are optimized numerically via the gradient-based method. With the discriminator and adversarial loss from GAN, VAEGAN model performs slightly better than VAE in reconstruction. It should be pointed out that all the three parameterization methods have small reconstruction MSEs of magnitude  $10^{-4}$ , meaning all the features extracted well encodes the airfoil shapes from the UIUC database.

**Table 1 Mean squared error of airfoil reconstruction via different featurization techniques**

Featurization	PCA	VAE	VAEGAN
MSE	$1.29208 \times 10^{-4}$	$3.70018 \times 10^{-4}$	$3.65345 \times 10^{-4}$

## B. Clustering in Feature Domain

The encoded features obtained from the encoder in our method can help better understand the shape of current airfoils. All airfoils from the UIUC Coordinate Database are first mapped to feature vectors, and an unsupervised learning algorithm, K-Means [58], is used to cluster these airfoils in the feature domain. To visualize the 32-dimensional feature domain, we use Parametric t-distributed Stochastic Neighbor Embedding (parametric t-SNE) [59, 60] as a visualization tool. Parametric t-SNE is modeled by MLP, which maps the high dimensional feature vector  $z_i$  into a low-dimension embedding  $y_i$ , while keeps the similarity between points. It converts similarities between data points to joint probabilities and minimizing the KL divergence between the joint probabilities of embedding  $y_i$  and the original feature vector  $z_i$ . Eq. 14 shows the cost function  $C$ , which t-SNE is expected to minimize:

$$\begin{aligned}
 p_{j|i} &= \frac{\exp(-\|z_i - z_j\|^2/2\sigma_i^2)}{\sum_{k \neq i} \exp(-\|z_i - z_k\|^2/2\sigma_i^2)}, \quad q_{j|i} = \frac{\exp(-\|y_i - y_j\|^2/2\sigma_i^2)}{\sum_{k \neq i} \exp(-\|y_i - y_k\|^2/2\sigma_i^2)}, \\
 C = KL(P||Q) &= \sum_i \sum_j p_{j|i} \log \frac{p_{j|i}}{q_{j|i}},
 \end{aligned} \tag{14}$$

where  $\sigma_i$  is calculated by a binary search given a fixed perplexity that is specified by the user [59]. Fig. 4 shows the K-means clustering results visualized with parametric t-SNE, where different colors represent different clusters, and the centroid of each cluster is also shown. The centroid of each cluster is different from each other in symmetry, height, camber, etc., and each represents the geometric pattern of each cluster. Features from close clusters represent similar airfoil shapes. The distance between feature points intuitively reflects the difference between the two airfoil shapes. This indicates that our VAEGAN-based model learns features that maintain the similarity of input airfoil shapes.

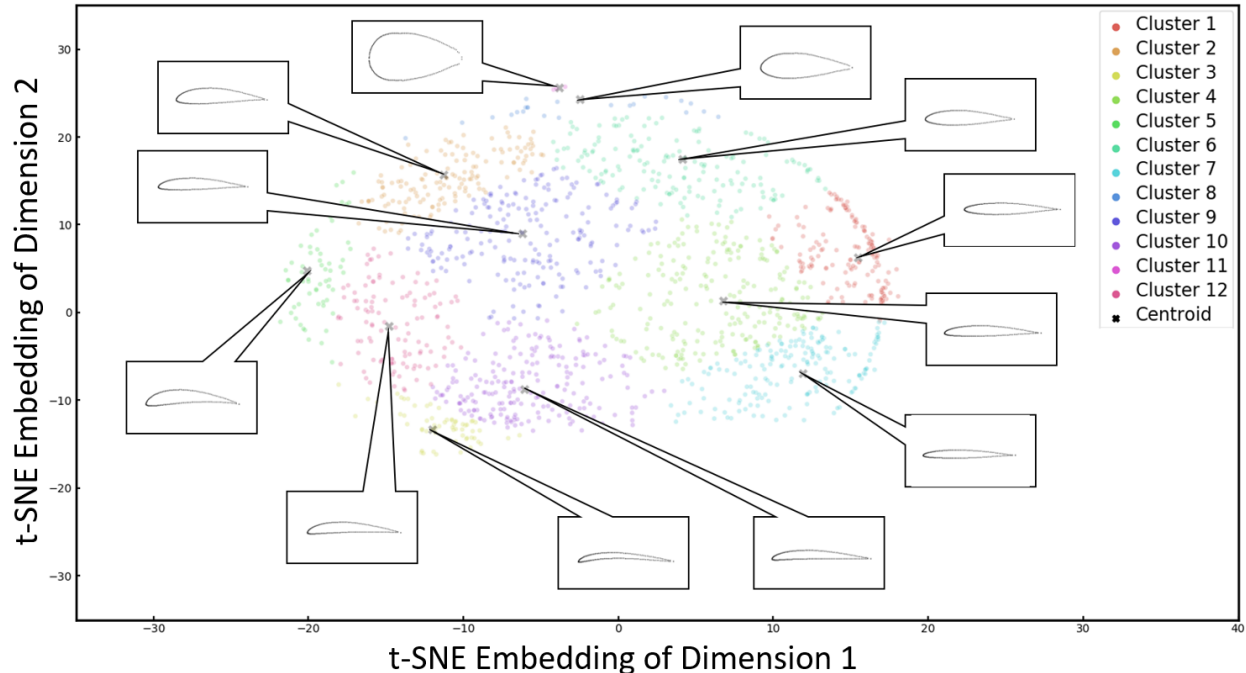


**Fig. 4 Parametric t-SNE visualization for clustering on feature domain**

### C. What is Encoded in the Feature Domain

Also, experiments are conducted to investigate what geometric features are encoded in each dimension of the learned representation. A series of manually designed feature vectors are fed into the decoder, where all the elements are set to zero except for one specific dimension. That particular element is changed gradually from  $-10$  to  $10$ , and the designed feature vectors are mapped to the airfoil coordinate domain by the decoder. Changes of generated airfoils are illustrated in Fig 5, and the 2D embedding of feature vectors using parametric t-SNE is shown in Fig 7. Here, only four dimensions are chosen for analysis purposes.

The 1<sup>st</sup> dimension encodes the height of the upper boundary, as illustrated in Fig 5a. As the 1<sup>st</sup> dimension increasing from  $-10$  to  $10$ , the height of the front half airfoil increases while the tail becomes thinner. The 8<sup>th</sup> dimension encodes the camber of both the upper boundary and the lower boundary. It is shown that by tuning the 8<sup>th</sup> dimension, the upper boundary of the airfoil changes from a concave curve to a horizontal straight line, while the lower boundary evolves

from a concave to a convex curve. Interestingly, the 22<sup>nd</sup> dimension encodes quite similar representations as the 1<sup>st</sup> dimension while in the opposite direction. In other words, generated airfoils from feature vectors whose 22<sup>nd</sup> dimension change from  $-10$  to  $10$  are like those with the 1<sup>st</sup> dimension change from  $10$  to  $-10$  as illustrated in Fig 7a and Fig 7c. Besides, Fig 5d shows how the last dimension is connected to the camber of the lower boundary. In detail, the curvature of the lower boundary decreases as the 32<sup>nd</sup> dimension increases.

In comparison to the features learned by our VAEGAN-based model, Fig. 6 shows the VAE-synthesized airfoils when changing only one feature dimension. As shown in 6a, the first dimension of VAE features fails to encode any shape representations. Even in the dimensions where representations are learned as dimension 3 and 31 shown in Fig. 6b and Fig. 6c, the feature does not change continuously as we observe in the VAEGAN results. Our VAEGAN-based model learns more representative and thorough features than the VAE model. Also, the representations in each dimension are entangled, like the 3<sup>rd</sup> dimension encodes both the upper bound and lower bound. These results indicate that, without manually designed parameters, our VAEGAN-based model learns geometrically meaningful features, and each dimension of the learned feature domain encodes informative and different geometry features.

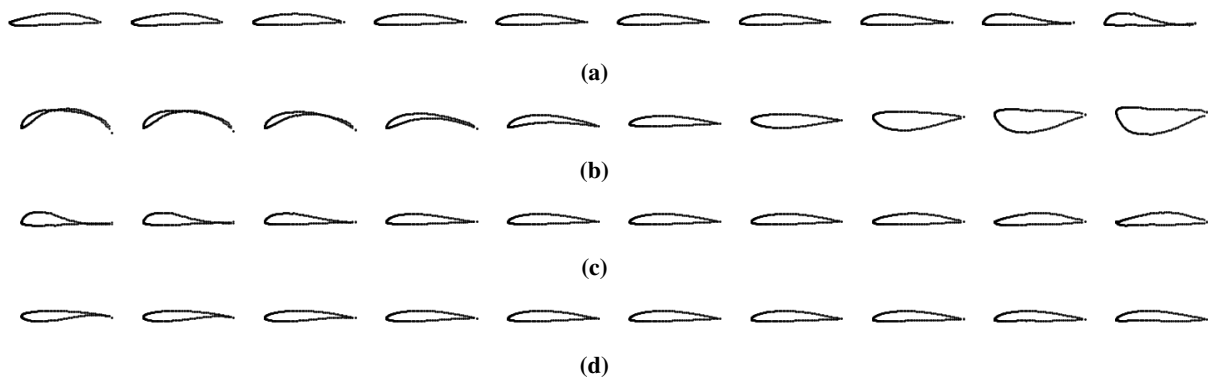


**Fig. 5** VAEGAN-generated airfoils by gradually changing only one dimension of the feature domain: (a) changes the 1<sup>st</sup> dimension, (b) changes the 8<sup>th</sup> dimension, (c) changes the 22<sup>nd</sup> dimension, and (d) changes the 32<sup>nd</sup> dimension

#### D. Synthesizing Novel Airfoils

To make use of the encoder-decoder architecture to synthesize novel airfoils, we conduct experiments on interpolation and extrapolation of feature vectors obtained from the UIUC Database airfoils as well as sampling from random Gaussian noises following the method introduced in Section III C.

As given in Eq. 9, the affine combination of two feature vectors,  $z_1$  and  $z_2$ , are computed with  $\nu = 0.5$ . Fig 8 shows the interpolated airfoils from two different clusters. The labels under each airfoil indicate which two clusters are  $z_1$  and  $z_2$  come from. As illustrated in Fig 8, the interpolated airfoil inherits features from both clusters. For instance, Cluster 6 and Cluster 11 both represent symmetric airfoil but with variant heights. The interpolation between these two clusters

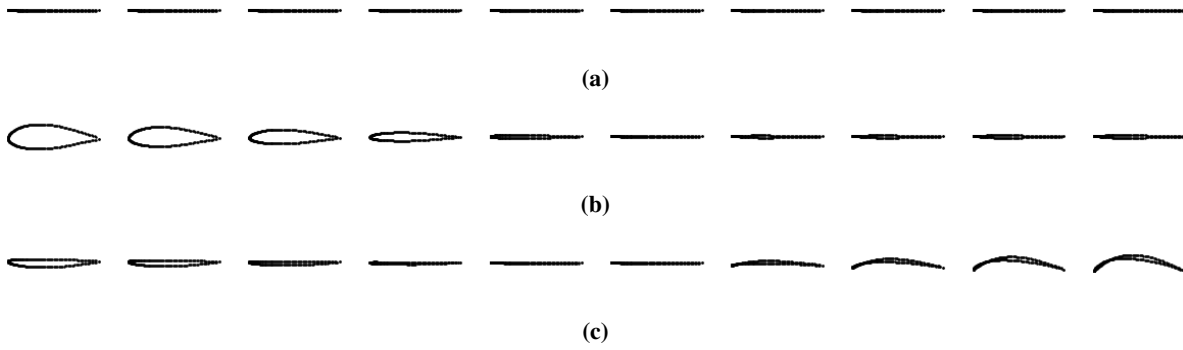


**Fig. 6** VAE-generated airfoils by gradually changing only one dimension of the feature domain: (a) change the 1<sup>st</sup> dimension, (b) changes the 3<sup>rd</sup> dimension, and (c) changes the 31<sup>st</sup> dimension

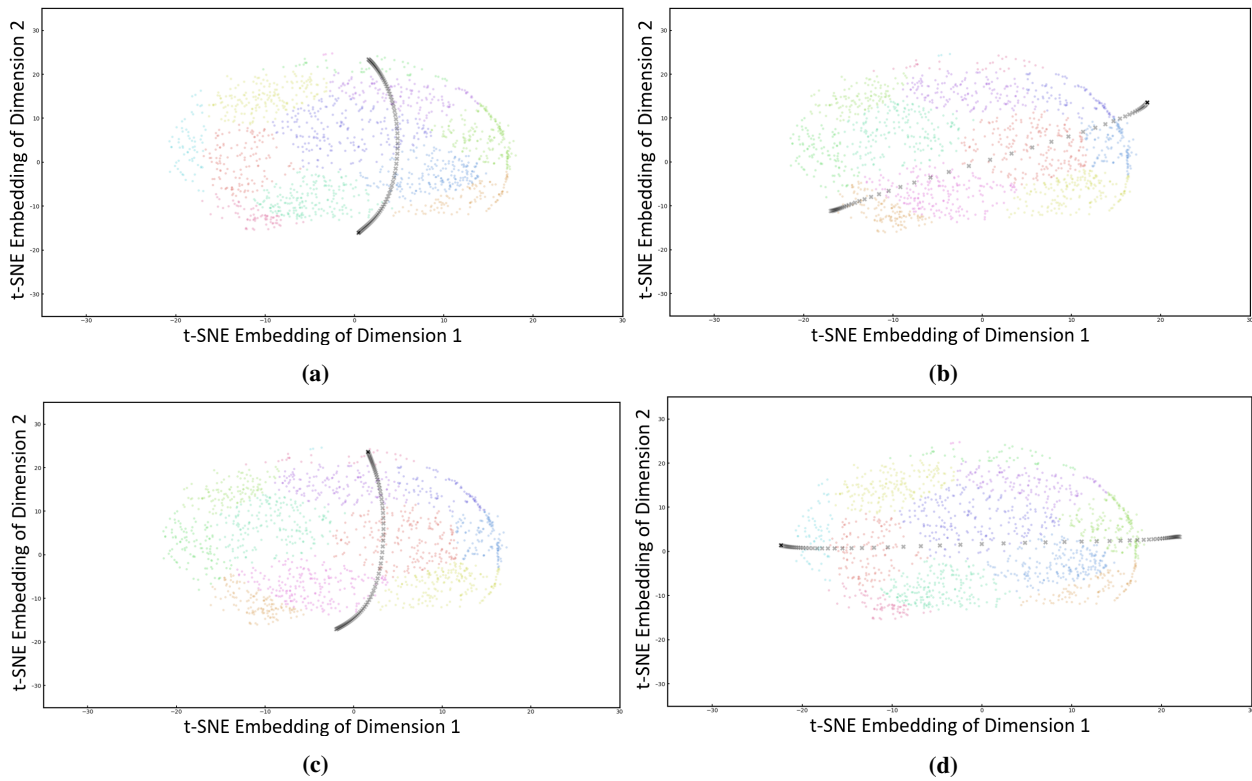


**Fig. 7** Path visualization of gradually changed feature on 2D embedded space using parametric t-SNE: (a) changing the 1<sup>st</sup> dimension, (b) changing the 8<sup>th</sup> dimension, (c) changing the 22<sup>nd</sup> dimension, and (d) changing the 32<sup>nd</sup> dimension

synthesizes a symmetric airfoil with a medium height, as shown in the last airfoil of Fig 8. Also, Clusters 3 and 4 both encode thin airfoils. However, the lower boundary is concave in Cluster 3, while Cluster 4 represents a convex lower boundary making the airfoil symmetric in shape. The interpolation between these two generates a thin airfoil with a flat lower boundary, which is a combination of concave and convex curves. By interpolation, novel airfoils with features from different clusters can be generated. Extrapolation between airfoils from different clusters is conducted as well.

Following Eq. 9, two feature vectors,  $z_1$  and  $z_2$ , are encoded from two different airfoils, and coefficient  $\nu$  is set to be 2. Fig 9 shows the generated results from the extrapolation. Similar to interpolation, extrapolated airfoils inherit features from  $z_1$  and  $z_2$ .

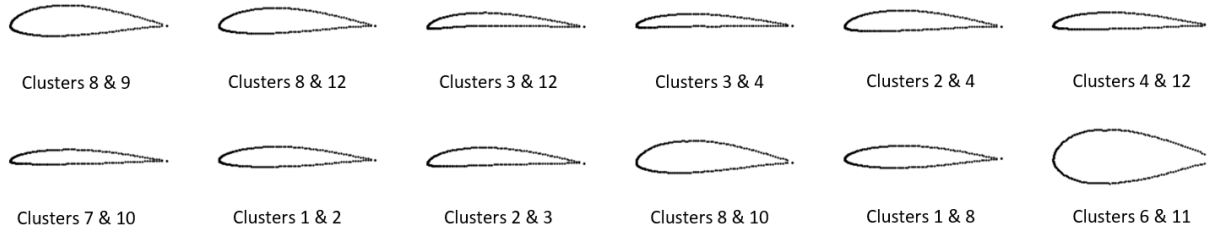


**Fig. 8 Interpolation of airfoils from different clusters**

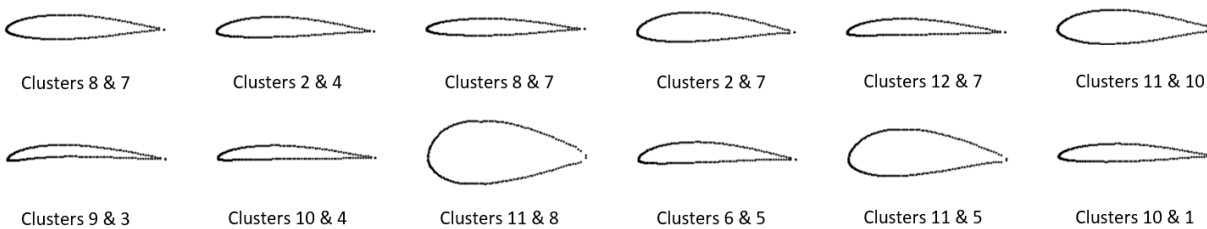


**Fig. 9 Extrapolation of airfoils from different clusters**

Besides interpolation and extrapolation, the performance of the sampling synthesis method is also estimated. In sampling, a Gaussian noise,  $\hat{z} \sim \mathcal{N}(0, \mathbf{I})$ , is directly fed into the decoder to generate novel airfoils. Shown in Fig. 10c are airfoils synthesized by our VAEGAN model through sampling. Besides, sampled airfoils using PCA and VAE are also included in Fig. 10a and Fig. 10b. PCA, as a linear projection technique, fails to synthesize realistic airfoils through random sampling. Both deep-learning-based generative models, VAE and VAEGAN, can synthesize different smooth airfoil shapes. To quantitatively measure the synthesized airfoils from VAE and VAEGAN, we here introduce Fréchet Inception Distance (FID) [61], which is used to evaluate the quality of samples from deep learning-based generative models. FID is calculated by computing the Fréchet distance between two feature representations. Generally, lower FID indicates higher generative sample quality. In our case, we feed the synthesized airfoils and the UIUC airfoils into the well-trained discriminator from VAEGAN and extract the second hidden layer as the representation. The FID for VAE and VAEGAN are 1.38788 and 0.65366, respectively, meaning VAEGAN synthesizes more realistic airfoils. Also, airfoils synthesized via VAEGAN possess more novelty while maintains the general geometric pattern of airfoils. For instance, in Fig. 10c, the first airfoils in the fourth row and the third one in the second row are different from existing samples in the UIUC database. Though such novelty does not guarantee better aerodynamic properties, some airfoils are likely to have negative lift coefficients, which are infeasible in practice. The VAEGAN-based model can synthesize a wide variety of airfoils that serve as candidates for further optimization through CFD simulation as we will investigate



in Section IV F.

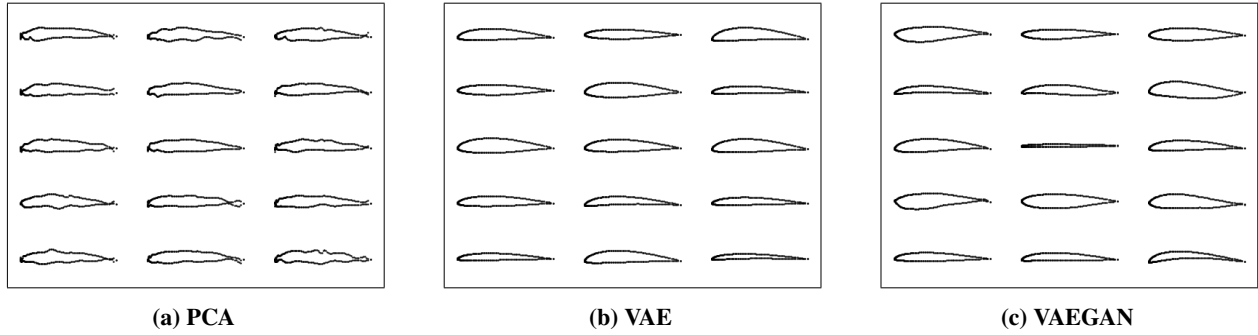


**Fig. 10** Generated airfoils by sampling with different featurization techniques.

### E. Aerodynamic Properties of Synthesized Airfoil

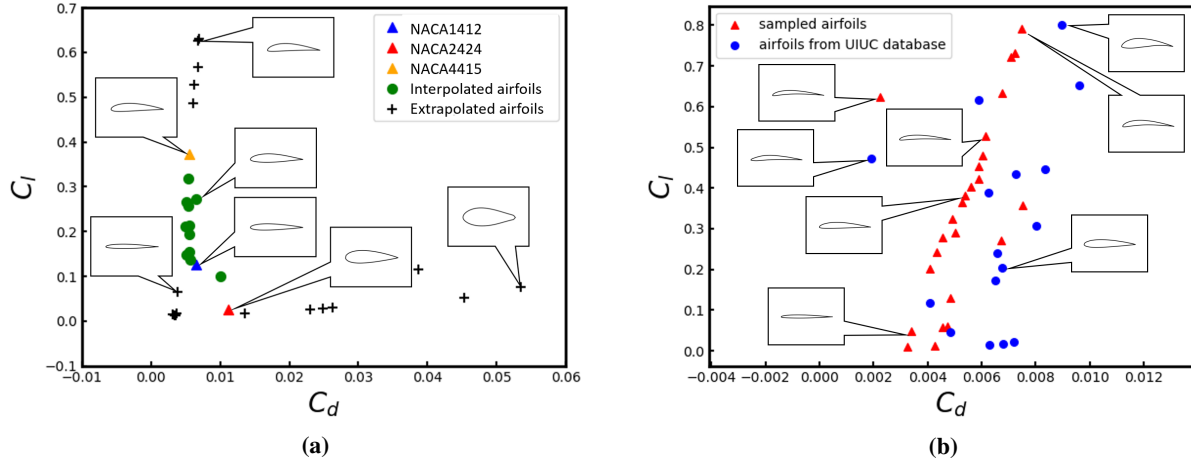


**Fig. 11** Lift coefficient  $C_l$  v.s. drag coefficient  $C_d$  of: (a) interpolated/extrapolated airfoils, and (b) sampled airfoils

Aerodynamic properties of the synthesized airfoils are also tested since airfoils have to meet certain aerodynamic properties to make the design feasible and effective. XFOIL\* is utilized to compute the lift coefficient,  $C_l$ , and the drag coefficient,  $C_d$ . The experiments on XFOIL is set for a low speed condition: Reynolds number  $Re = 2 \times 10^6$ , Mach number  $Ma = 0.02$ , and attack angle  $\alpha = 0^\circ$ . As illustrated in Fig 11a,  $C_l$  and  $C_d$  are tested on three airfoils: NACA1412, NACA2424 and NACA4415 from the UIUC database. Following Eq. 10, triplet interpolation/extrapolation is conducted with feature vectors,  $z_1$ ,  $z_2$ , and  $z_3$ , encoded from the three NACA airfoils. The interpolated airfoils, marked by green dots, possess  $C_l$  and  $C_d$  in between the three NACA airfoils. While extrapolated airfoils, marked by black crossings, have significantly different aerodynamic properties from the interpolated airfoils. Some airfoils synthesized by extrapolation have high  $C_l$  with relatively low  $C_d$ , located at the upper part of Fig. 11a. This demonstrates

\*<https://web.mit.edu/drela/Public/web/xfoil/>

that by interpolation/extrapolation in the feature domain, novel airfoils with promising aerodynamic properties can be synthesized. Also, aerodynamic properties of synthesized airfoils by sampling are tested in comparison with some airfoils from the UIUC database, as shown in Fig 11b. Though the generated airfoils from Gaussian noises are not guaranteed to have good aerodynamic properties, like red dots lying on the bottom left. Some promising airfoils can be synthesized, as shown on the top right, with a high lift coefficient and a low drag coefficient. By sampling, the VAEGAN-based model can synthesize airfoils with a wide variety of aerodynamic properties. Such a variety provides abundant candidates to explore in design space for airfoil shape optimization.

### F. Shape Optimization on Aerodynamic Properties via Genetic Algorithm

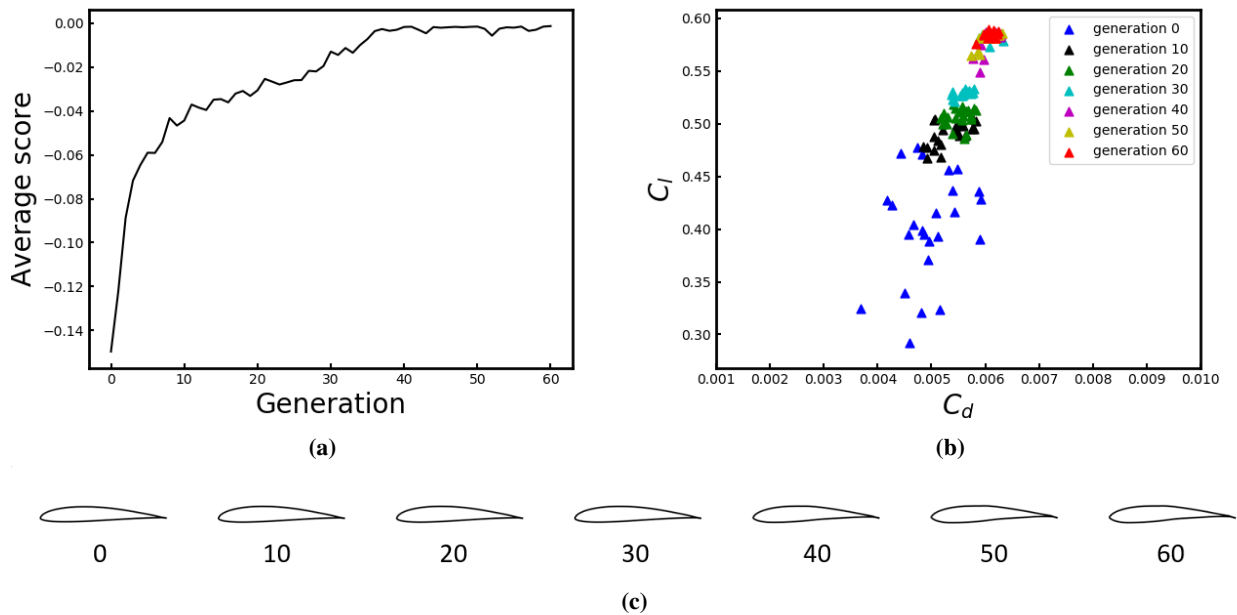


**Fig. 12 Shape optimization via genetic algorithm: (a) average score of each generation; (b)  $C_l$  and  $C_d$  of synthesized airfoils for different generations; (c) synthesized airfoil geometry for different generation**

The VAEGAN model has been proven to be able to parameterize existing airfoils to latent feature vectors and synthesize novel airfoils automatically. However, whether or not the learned features and synthesized airfoils can be optimized to possess desired aerodynamic properties remains untested. To this end, this section demonstrates that with the VAEGAN model, airfoil shapes can be optimized to realize the target  $C_l$  and  $C_d$  value via a genetic algorithm (GA). The lift and drag coefficients,  $C_l$  and  $C_d$ , calculated are under the same condition as Section IV E. As illustrated in Fig. 12, the target lift coefficient is  $C_l^t = 0.6$ , and target drag coefficient is  $C_d^t = 0.06$ . In our case, the total number of generations,  $N$ , is set to be 60, and the number of populations on each generation,  $M$ , to be 25. Fig. 12a and Fig. 12b show how the average score and  $C_l, C_d$  change with generation, respectively. As Fig. 12c illustrates, the airfoil shape gradually evolves to the target  $C_l$  and  $C_d$ . Also, we compare the performance of airfoil optimization using different featurization

techniques, PCA, and VAE. The genetic algorithm with the same objective function and settings are conducted. The lift coefficient  $C_l$ , drag coefficient  $C_d$ , and fitness score of the last generation in the genetic algorithm is reported in Table 2. The VAEGAN-synthesized airfoils reach an averaged lift coefficient of 0.5857 and an averaged drag coefficient of 0.0061. The coefficients are close to the desired aerodynamic properties. Whereas PCA and VAE fail to synthesize desired airfoils within the same number of generations and population size. This is because our VAEGAN-based model generates a wider variety of airfoils that serves as potential candidates in design optimization. Such experiments prove that a simple optimization technique like GA and the well-trained VAEGAN model can synthesize airfoils with desired aerodynamic properties, which can guide designing effective and efficient aerodynamic products.

**Table 2 Airfoil design optimization results with different featurization techniques**

Featurization	$C_l$		$C_d$		Fitness score	
	mean	std	mean	std	mean	std
PCA	0.41953	0.012672	0.0069430	$6.9231 \times 10^{-4}$	-0.12893	0.046250
VAE	0.52746	0.0017073	0.0056662	$1.4631 \times 10^{-5}$	-0.017819	0.0014068
VAEGAN	0.58570	0.0028946	0.0061030	$7.0711 \times 10^{-6}$	$-8.5312 \times 10^{-4}$	0.00089211

## V. Conclusion

In this work, a data-driven method is proposed to achieve three goals: (1) automatically featuring airfoil geometries from the UIUC Database [53] without manually designed parameters, (2) synthesizing novel airfoils by either interpolating or extrapolating the encoded features, as well as generating from random noise, and (3) optimizing the features to synthesize airfoils with desired aerodynamic properties. Our model is built upon VAEGAN, which combines the encoder-decoder architecture from VAE [6] [7] and the discriminator from GAN [8]. With the encoder-decoder structure, our model learns explicit mappings from airfoil coordinates to latent feature domain as well as from feature vectors to airfoils, while with the discriminator, the model can automatically synthesize realistic samples. Also, our model is trained in a self-supervised manner. Namely, the model learns compact and informative features directly from airfoil shapes without manually tagged labels or designed parameters. Optimized on the learned feature domain via GA, the synthesized airfoils can evolve to have desired aerodynamic properties.

Experiments show that our model learns compact and comprehensive features encoding shape information of airfoils and can automatically generate novel airfoils. First, airfoils can be reconstructed via decoding the learned features with minor error compared to the origin coordinates. Second, K-Means [58] clustering on the feature domain of the UIUC Coordinate Database further demonstrates the learned representations are meaningful in a way that the centroid of each cluster represents different shapes. It is also investigated what is encoded in each dimension of the feature domain by gradually changing the feature vector on one specific dimension with all other dimensions fixed. Without human prior, each dimension encodes different geometric information like height, camber, symmetry, and even coupled features.

Moreover, novel airfoils are synthesized by interpolating and extrapolating learned features from different airfoils as well as directly generated from random noise. By interpolating or extrapolating, the synthesized airfoil inherits and blends features from existing airfoils, which provides insights for designing new airfoils. On the other hand, airfoils generated from Gaussian noise are more aggressive in a way that they follow a less geometrical format of existing airfoils, and more novelty is introduced to the airfoil design. Finally, the synthesized airfoils can be optimized via GA to possess competitive or even better aerodynamic properties in comparison to existing ones, indicating the synthesized geometries are not only plausible in shape but also practical in aerodynamic performance.

## References

- [1] LeCun, Y., Bengio, Y., and Hinton, G., “Deep learning,” *Nature*, Vol. 521, No. 7553, 2015, p. 436.
- [2] Voulodimos, A., Doulamis, N., Doulamis, A., and Protopapadakis, E., “Deep learning for computer vision: A brief review,” *Computational intelligence and neuroscience*, Vol. 2018, 2018.
- [3] Cambria, E., and White, B., “Jumping NLP curves: A review of natural language processing research,” *IEEE Computational intelligence magazine*, Vol. 9, No. 2, 2014, pp. 48–57.
- [4] Pierson, H. A., and Gashler, M. S., “Deep learning in robotics: a review of recent research,” *Advanced Robotics*, Vol. 31, No. 16, 2017, pp. 821–835.
- [5] Carrio, A., Sampedro, C., Rodriguez-Ramos, A., and Campoy, P., “A review of deep learning methods and applications for unmanned aerial vehicles,” *Journal of Sensors*, Vol. 2017, 2017.
- [6] Kingma, D. P., and Welling, M., “Auto-encoding variational bayes,” *arXiv preprint arXiv:1312.6114*, 2013.
- [7] Rezende, D. J., Mohamed, S., and Wierstra, D., “Stochastic backpropagation and approximate inference in deep generative models,” *arXiv preprint arXiv:1401.4082*, 2014.
- [8] Goodfellow, I., Pouget-Abadie, J., Mirza, M., Xu, B., Warde-Farley, D., Ozair, S., Courville, A., and Bengio, Y., “Generative adversarial nets,” *Advances in neural information processing systems*, 2014, pp. 2672–2680.
- [9] Karras, T., Laine, S., and Aila, T., “A style-based generator architecture for generative adversarial networks,” *Proceedings of the IEEE Conference on Computer Vision and Pattern Recognition*, 2019, pp. 4401–4410.
- [10] Samareh, J. A., “Survey of shape parameterization techniques for high-fidelity multidisciplinary shape optimization,” *AIAA journal*, Vol. 39, No. 5, 2001, pp. 877–884.
- [11] Chang, K.-H., and Chen, C., “3D shape engineering and design parameterization,” *Computer-Aided Design and Applications*, Vol. 8, No. 5, 2011, pp. 681–692.
- [12] Salunke, N. P., Juned Ahamad, R., and Channiwalla, S., “Airfoil parameterization techniques: A review,” *American Journal of Mechanical Engineering*, Vol. 2, No. 4, 2014, pp. 99–102.

- [13] Abbott, I. H., Von Doenhoff, A. E., and Stivers Jr, L., “Summary of airfoil data,” 1945.
- [14] Rajnarayan, D., Haas, A., and Kroo, I., “A multifidelity gradient-free optimization method and application to aerodynamic design,” *12th AIAA/ISSMO multidisciplinary analysis and optimization conference*, 2008, p. 6020.
- [15] Sederberg, T. W., and Farouki, R. T., “Approximation by interval Bézier curves,” *IEEE Computer Graphics and Applications*, , No. 5, 1992, pp. 87–88.
- [16] Derksen, R., and Rogalsky, T., “Bezier-PARSEC: An optimized aerofoil parameterization for design,” *Advances in engineering software*, Vol. 41, No. 7-8, 2010, pp. 923–930.
- [17] Larsen, A. B. L., Sønderby, S. K., Larochelle, H., and Winther, O., “Autoencoding beyond pixels using a learned similarity metric,” *arXiv preprint arXiv:1512.09300*, 2015.
- [18] Mitchell, M., *An introduction to genetic algorithms*, MIT Press, 1998.
- [19] Hicks, R. M., and Henne, P. A., “Wing design by numerical optimization,” *Journal of Aircraft*, Vol. 15, No. 7, 1978, pp. 407–412.
- [20] HAGER, J., Eyi, S., and Lee, K., “A multi-point optimization for transonic airfoil design,” *4th Symposium on Multidisciplinary Analysis and Optimization*, 1992, p. 4681.
- [21] Sobieczky, H., “Geometry generator for CFD and applied aerodynamics,” *New Design Concepts for High Speed Air Transport*, Springer, 1997, pp. 137–157.
- [22] Elliott, J., and Peraire, J., “Practical three-dimensional aerodynamic design and optimization using unstructured meshes,” *AIAA Journal*, Vol. 35, No. 9, 1997, pp. 1479–1485.
- [23] TAYLOR, A., III, HOU, G., and KORIVI, V., “Sensitivity analysis, approximate analysis, and design optimization for internal and external viscous flows,” *Aircraft Design and Operations Meeting*, 1991, p. 3083.
- [24] Boehm, W., and Müller, A., “On de Casteljau’s algorithm,” *Computer Aided Geometric Design*, Vol. 16, No. 7, 1999, pp. 587–605.
- [25] Farin, G., *Curves and surfaces for computer-aided geometric design: a practical guide*, Elsevier, 2014.
- [26] Sederberg, T. W., and Parry, S. R., “Free-form deformation of solid geometric models,” *ACM SIGGRAPH computer graphics*, Vol. 20, No. 4, 1986, pp. 151–160.
- [27] Coquillart, S., *Extended free-form deformation: a sculpturing tool for 3D geometric modeling*, Vol. 24, ACM, 1990.
- [28] Yeh, T.-P., and Vance, J. M., “Applying virtual reality techniques to sensitivity-based structural shape design,” *Journal of Mechanical Design*, Vol. 120, No. 4, 1998, pp. 612–619.

- [29] Li, J., Bouhlel, M. A., and Martins, J. R., "Data-based approach for fast airfoil analysis and optimization," *AIAA Journal*, Vol. 57, No. 2, 2019, pp. 581–596.
- [30] Poole, D. J., Allen, C. B., and Rendall, T., "Efficient Aero-Structural Wing Optimization Using Compact Aerofoil Decomposition," *AIAA Scitech 2019 Forum*, 2019, p. 1701.
- [31] LeCun, Y., Boser, B., Denker, J. S., Henderson, D., Howard, R. E., Hubbard, W., and Jackel, L. D., "Backpropagation applied to handwritten zip code recognition," *Neural computation*, Vol. 1, No. 4, 1989, pp. 541–551.
- [32] LeCun, Y., Bottou, L., Bengio, Y., Haffner, P., et al., "Gradient-based learning applied to document recognition," *Proceedings of the IEEE*, Vol. 86, No. 11, 1998, pp. 2278–2324.
- [33] Szegedy, C., Liu, W., Jia, Y., Sermanet, P., Reed, S., Anguelov, D., Erhan, D., Vanhoucke, V., and Rabinovich, A., "Going deeper with convolutions," *Proceedings of the IEEE conference on computer vision and pattern recognition*, 2015, pp. 1–9.
- [34] He, K., Zhang, X., Ren, S., and Sun, J., "Delving deep into rectifiers: Surpassing human-level performance on imagenet classification," *Proceedings of the IEEE international conference on computer vision*, 2015, pp. 1026–1034.
- [35] Ren, S., He, K., Girshick, R., and Sun, J., "Faster r-cnn: Towards real-time object detection with region proposal networks," *Advances in neural information processing systems*, 2015, pp. 91–99.
- [36] Redmon, J., Divvala, S., Girshick, R., and Farhadi, A., "You only look once: Unified, real-time object detection," *Proceedings of the IEEE conference on computer vision and pattern recognition*, 2016, pp. 779–788.
- [37] Li, Y., Qi, H., Dai, J., Ji, X., and Wei, Y., "Fully convolutional instance-aware semantic segmentation," *Proceedings of the IEEE Conference on Computer Vision and Pattern Recognition*, 2017, pp. 2359–2367.
- [38] He, K., Gkioxari, G., Dollár, P., and Girshick, R., "Mask r-cnn," *Proceedings of the IEEE international conference on computer vision*, 2017, pp. 2961–2969.
- [39] Norgaard, M., Jorgensen, C. C., and Ross, J. C., "Neural network prediction of new aircraft design coefficients," 1997.
- [40] Zhang, Y., Sung, W. J., and Mavris, D. N., "Application of convolutional neural network to predict airfoil lift coefficient," *2018 AIAA/ASCE/AHS/ASC Structures, Structural Dynamics, and Materials Conference*, 2018, p. 1903.
- [41] Yilmaz, E., and German, B., "A convolutional neural network approach to training predictors for airfoil performance," *18th AIAA/ISSMO Multidisciplinary Analysis and Optimization Conference*, 2017, p. 3660.
- [42] Yilmaz, E., and German, B., "A deep learning approach to an airfoil inverse design problem," *2018 Multidisciplinary Analysis and Optimization Conference*, 2018, p. 3420.
- [43] Arjovsky, M., Chintala, S., and Bottou, L., "Wasserstein gan," *arXiv preprint arXiv:1701.07875*, 2017.
- [44] Mirza, M., and Osindero, S., "Conditional generative adversarial nets," *arXiv preprint arXiv:1411.1784*, 2014.

- [45] Chen, X., Duan, Y., Houthoofd, R., Schulman, J., Sutskever, I., and Abbeel, P., “Infogan: Interpretable representation learning by information maximizing generative adversarial nets,” *Advances in neural information processing systems*, 2016, pp. 2172–2180.
- [46] Radford, A., Metz, L., and Chintala, S., “Unsupervised representation learning with deep convolutional generative adversarial networks,” *arXiv preprint arXiv:1511.06434*, 2015.
- [47] Chen, W., and Fuge, M., “B\`ezierGAN: Automatic Generation of Smooth Curves from Interpretable Low-Dimensional Parameters,” *arXiv preprint arXiv:1808.08871*, 2018.
- [48] Chen, W., Chiu, K., and Fuge, M., “Aerodynamic Design Optimization and Shape Exploration using Generative Adversarial Networks,” *AIAA Scitech 2019 Forum*, 2019, p. 2351.
- [49] Wu, J., Zhang, C., Xue, T., Freeman, B., and Tenenbaum, J., “Learning a probabilistic latent space of object shapes via 3d generative-adversarial modeling,” *Advances in neural information processing systems*, 2016, pp. 82–90.
- [50] Huang, H., Kalogerakis, E., and Marlin, B., “Analysis and synthesis of 3D shape families via deep-learned generative models of surfaces,” *Computer Graphics Forum*, Vol. 34, Wiley Online Library, 2015, pp. 25–38.
- [51] Sinha, A., Unmesh, A., Huang, Q., and Ramani, K., “Surfnets: Generating 3d shape surfaces using deep residual networks,” *Proceedings of the IEEE conference on computer vision and pattern recognition*, 2017, pp. 6040–6049.
- [52] Kalogerakis, E., Chaudhuri, S., Koller, D., and Koltun, V., “A probabilistic model for component-based shape synthesis,” *ACM Transactions on Graphics (TOG)*, Vol. 31, No. 4, 2012, p. 55.
- [53] Selig, M., *UIUC airfoil data site*, Department of Aeronautical and Astronautical Engineering University of Illinois at Urbana-Champaign, 1996.
- [54] Poon, P. W., and Carter, J. N., “Genetic algorithm crossover operators for ordering applications,” *Computers & Operations Research*, Vol. 22, No. 1, 1995, pp. 135–147.
- [55] Maas, A. L., Hannun, A. Y., and Ng, A. Y., “Rectifier nonlinearities improve neural network acoustic models,” *Proc. icml*, Vol. 30, 2013, p. 3.
- [56] Kingma, D. P., and Ba, J., “Adam: A method for stochastic optimization,” *arXiv preprint arXiv:1412.6980*, 2014.
- [57] Schafer, R. W., et al., “What is a Savitzky-Golay filter,” *IEEE Signal processing magazine*, Vol. 28, No. 4, 2011, pp. 111–117.
- [58] Jain, A. K., “Data clustering: 50 years beyond K-means,” *Pattern recognition letters*, Vol. 31, No. 8, 2010, pp. 651–666.
- [59] Maaten, L. v. d., and Hinton, G., “Visualizing data using t-SNE,” *Journal of machine learning research*, Vol. 9, No. Nov, 2008, pp. 2579–2605.
- [60] Van Der Maaten, L., “Learning a parametric embedding by preserving local structure,” *Artificial Intelligence and Statistics*, 2009, pp. 384–391.

- [61] Heusel, M., Ramsauer, H., Unterthiner, T., Nessler, B., and Hochreiter, S., “Gans trained by a two time-scale update rule converge to a local nash equilibrium,” *Advances in neural information processing systems*, 2017, pp. 6626–6637.